Mitigation of ELMs and Disruptions by Pellet Injection

K. Gál 1), T. Fehér 1), T. Fülöp 2), P. T. Lang 3), H. M. Smith 4), ASDEX Upgrade Team 5) and JET-EFDA contributors 3)

1) KFKI-RMKI, Association EURATOM, Budapest, Hungary
2) Chalmers University of Technology and Euratom-VR Association, Sweden
3) EFDA-JET, Culham Science Centre, OX14 3DB, Abingdon, OXON, United Kingdom
4) Centre for Fusion, Space and Astrophysics, University of Warwick, Coventry, UK
5) Max-Planck-Institut für Plasmaphysik, Garching, Germany

e-mail contact of main author: gal@rmki.kfki.hu

Abstract
Deuterium, impurity and impurity doped pellets are studied in light of their use for ELM and disruption mitigation. Based on ELM pace making studies at ASDEX Upgrade and JET, the minimum pellet size required to cause an ELM, has been estimated in ITER for the foreseen pellet velocities. Concerning disruption mitigation studies the number of runaways is determined for JET like plasmas for deuterium, carbon and carbon-doped deuterium pellets. To calculate the ablation rate and to describe the cloud dynamics we used the Hybrid code which considers the formation of the neutral cloud according to the NGS ablation model and the dynamics of the ionized cloud part is treated by an one-dimensional Lagrangian cell code. Interaction between cold pellet particles and background plasma, radiation, Ohmic heating and heat diffusion are taken into account to calculate the change in the background plasma temperature. The resistive diffusion of the electric field is followed, and the resulting number of Dreicer, hot-tail and avalanche runaway electrons are calculated during the current quench. This way a tool has been created to test the suitability of different pellets for disruption mitigation.

1. Introduction

Heat loads caused by disruptions and ELMs may severely damage fusion devices [1]. For disruptions, halo currents and runaway electrons are also a serious problem. Several methods have been proposed to mitigate both ELMs and disruptions, one of them is pellet injection [2, 3]. ELMs are triggered by deuterium pellets reaching the pedestal top. Disruptions can be mitigated by strongly radiating impurity pellets. The present work aims at studying deuterium, impurity and impurity doped pellets in the light of their use for ELM and disruption mitigation.

To understand how a pellet can trigger an ELM or mitigate a disruption one needs to know how different pellets ablate. Due to the low sublimation energy (5meV/particle), and relatively high ionization energy (13.6eV) of deuterium a spherically expanding neutral cloud forms once the pellet enters the plasma. This cloud will turn into a channel flow as the particles become ionized at the cloud periphery (i.e. at the cloud radius). In the case of impurities such as carbon, the role of the neutral cloud part is reduced, as the difference between the sublimation (4-8eV) and ionization energy ($C \rightarrow C^+$ 11.2eV) is less pronounced.

Simulations of pellet ablation and cloud expansion were performed employing a hybrid code [4], which describes the spherical neutral cloud according to the neutral gas shielding (NGS) model [5], while the detailed dynamics of the field line elongated ionized cloud is exploited by a one-dimensional Lagrangian cell code [6].

For low velocity deuterium pellets the shielding effect of the ionized cloud part plays a significant role, while in the high velocity limit it becomes negligible. The shielding effect decreases with speed because it correlates with the amount of material deposited during the time interval the pellet spends in its cloud (flux tube). Consequently, it is not only important for low velocities, but also for large pellet sizes to properly model the ionized cloud. For example, the hybrid code gives a 30% lower ablation rate than the NGS model (which does not include the ionized cloud) as can be seen on the occasion of a 1 mm pellet in Fig. 1. Therefore, the hybrid code was applied for all simulations of deuterium and carbon doped deuterium pellets. In ITER the expected pellet velocities range from 300 to 500 m/s [7] and the pellet radius will be much greater than 1 mm, so the effects of the ionized pellet cloud can be more important than for pellets used in present devices. It should be emphasized here that this effect can be reduced by drifts.

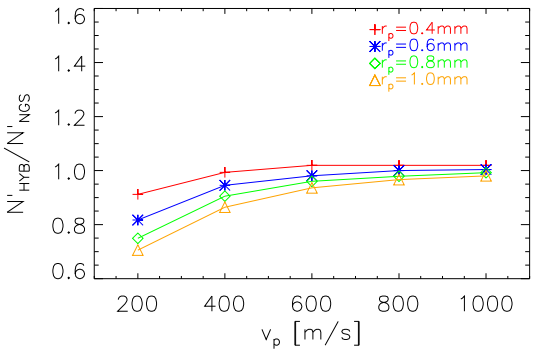

FIG. 1: The ratio of the hybrid and NGS ablation rates as a function of velocity. The target plasma temperature is 800 eV *and density is* $2 \cdot 10^{19}$ m^{-3}.

2. Effects in the fast time domain

Simulation were performed in connection with ELM triggering experiments performed at ASDEX Upgrade [2] and JET [8]. In both machines all injected pellets trigger an ELM before the pellet reaches the pedestal top, although different pellets induced different density perturbations (deposited particles/m). The minimum perturbation is caused by the fastest and smallest technically available pellet. In ASDEX Upgrade this is a 1000 m/s and 0.5 mm pellet causing a perturbation of $\sim 2 \cdot 10^{20}$ m^{-1} in the pedestal region (middle of the pedestal). For JET experiments, high resolution data are only available for high field side injection, so a simulation was performed for such a case [8]. The pellet mass was taken to be the same as in the experiment (yielding 2.45 mm radius), while its radial velocity was 115 m/s. The perturbation strength was found to be $8 \cdot 10^{20}$ /m in this simulation.

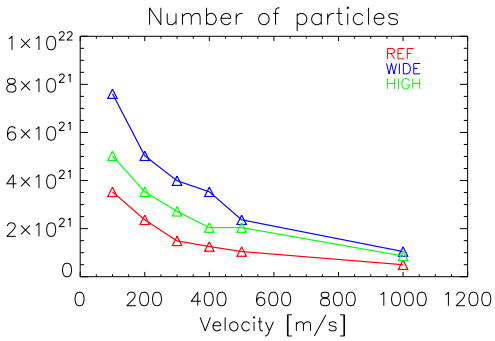

FIG. 2: The size of the pellet (number of deuterons) required to reach the ITER pedestal top as a function of the velocity for LFS injection line.

As all these pellets trigger ELMs we can conclude that the above calculated perturbation strength ($\sim 10^{20}$ /m) is enough to trigger ELMs in ASDEX Upgrade and in JET. The pellet velocities in ITER are foreseen to be similar to the ones used at JET and ASDEX Upgrade, so the minimum density perturbation strength can also be assumed to be of the same order as in these two machines. First we assumed that every pellet reaching the ITER pedestal top triggers an ELM, therefore we calculated the particle content of such pellets. The simulations were performed for thee typical pellet injection scenarios with "Reference pedestal" (pedestal temperature: 4keV, width along the pellet path:

10cm), "High pedestal" (pedestal temperature: 5keV, width along the pellet path: 10cm) and "Wide pedestal" (pedestal temperature: 4keV, width along the pellet path: 20cm). The particle content of pellets having 300m/s and 500m/s velocity was of the order of $1 - 4 \cdot 10^{21}$ deuterons (see Fig. 2). For all the simulated ITER pellets in Fig. 2 the perturbation strength is in the order of 10^{21} /m, larger than in ASDEX Upgrade and JET. If the pellet induced perturbation triggering an ELM is measured by the number of deposited particles per meter, than all pellets in Fig. 2 will trigger an ELM in ITER.
In contrast to our expectations that ELM triggering efficiency depends on density perturbation strength, detailed experiments at ASDEX Upgrade [9] showed that there is no correlation between the strength of the pellet induced MHD perturbation (measured by Mirnov coils etc) and the number of ablated or deposited particles. The magnitude of the perturbation signal only correlates with the pellet position in the plasma. This would indicate that the strength of the pellet induced perturbation is above the saturation level of ELM triggering, if the scenario is prone to ELMs, therefore a well defined lower density limit for ELM triggering cannot be given in this way.

Besides particle deposition, the pellet induces a perturbation by cooling. On a short time scale ($\sim 10\mu s$) the pellet cools the plasma by energy absorption consumed for ablation and cloud formation. This initial cooling is followed by a temperature decrease due to the dilution of the pellet particles in the background plasma. On a longer time scale we modeled the temperature evolution of the plasma with energy balance equations.

As the pellet travels into the plasma it ablates and forms consecutive cylindrical clouds. In the first phase the temperature of the background plasma, T_e^{bg} is decreased due to heat absorption by the cloud [10]. This energy is extracted from a flux shell containing the cloud. Such a flux shell is bounded by two nearby flux surfaces, separated radially by a distance equal to the cloud diameter ($2R_{cld}$), and its volume is denoted by V_{flt}. The heat is absorbed at the cloud periphery:

$$\frac{d}{dt}\left[\frac{3}{2}n_e^{bg}T_e^{bg}V_{flt}\right] = -2\pi R_{cld}q_{\parallel}(R_{cld} + z_{cld}\cdot q_{\perp}/q_{\parallel}), \quad (1)$$

where z_{cld} is the toroidal cloud extension and n_e^{bg} is the density of the background plasma. The quantities $q_{\parallel}$ and $q_{\perp}$ are the parallel and perpendicular heat fluxes ($q_{\perp}/q_{\parallel} \sim 5\%$). The field elongated size of the cloud is important, since it determines the heat absorption in the perpendicular direction. The perpendicular heat absorption is especially important for impurity or impurity doped pellets, which produce relatively long clouds, while it is negligible for deuterium pellets, which give shorter clouds.

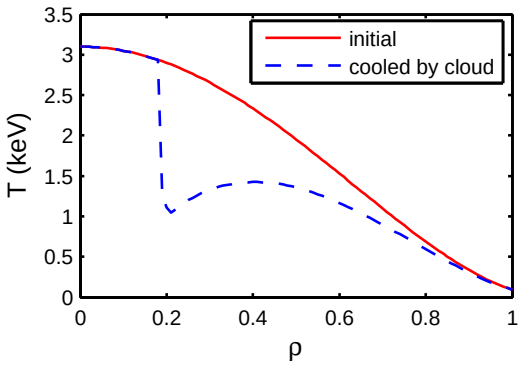

FIG. 3: Temperature decrease due a deuterium pellet with $r_p = 3$ mm ($6.8 \cdot 10^{21}$ particles) and $v_p = 160$ m/s.

Once the pellet leaves its cigar shaped cloud (flux tube) and forms another one, the particles from the pellet cloud will spread out over the flux surface and the density (n_e) increase is estimated by simply summing up the number of the electrons:

$$n_e V_{flt} = n_e^{bg}(V_{flt} - V_{cld}) + n_e^{cld}V_{cld}. \quad (2)$$

where V_{cld} and n_{cld} are the volume and the density of the cloud. Here we should note that

particles might be moved from the cloud or from the flux surface by drift effects etc, but these effects are neglected in the present work.
The flux surface averaged temperature is estimated by energy conservation:

$$n_e T_e V_{flt} = n_e^{bg} T_e^{bg} (V_{flt} - V_{cld}) + n_e^{cld} T_e^{cld} V_{cld}. \quad (3)$$

In the plasma edge, the deuterium pellet induced flux surface averaged cooling is low even for a large pellet (see Fig. 3), but the local, toroidally asymmetric cooling can be higher close to the pellet, which might contribute to ELM formation. The present approach cannot give a clear answer to how the pellet induced cooling contributes to ELM formation.

The plasma cooling effect is especially important when the injected pellet is used for disruption mitigation. For deuterium pellets the absorbed heat is mainly consumed by cloud expansion, while in the case of carbon and carbon doped deuterium pellets it is radiated. Already in the first part of the cooling process, when heat transport issues can be neglected, the energy absorption from the background plasma is higher for impurity or impurity doped pellets than for deuterium pellets. The time dependence of the plasma density (sum of the electrons in the cloud and of the background plasma) and temperature is shown in Fig. 4, emphasizing the difference between deuterium, carbon and carbon doped deuterium pellets.

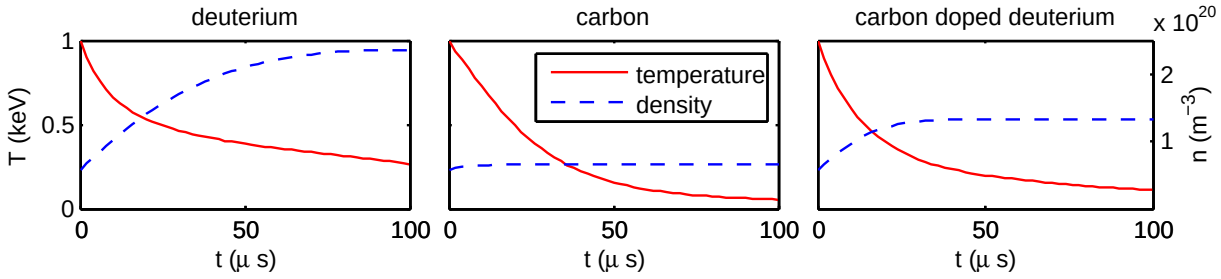

FIG. 4: The electron temperature and density evolution induced by deuterium, carbon and carbon doped deuterium pellets (1% carbon) with $r_p = 0.9$ mm and $v_p = 200$ m/s.

3. Long term issues

For disruption mitigation scenarios, it is important to model what happens on the longer time scale of the current quench, which can even be of the order of seconds. During and after the flux surface homogenization, the background plasma evolution can be described by the energy balance equations for pellet ions (p), deuterons (D) and electrons (e):

$$\frac{3}{2}\frac{\partial(n_e T_e)}{\partial t} = \frac{3n_e}{2r}\frac{\partial}{\partial r}\left(\chi\, r \frac{\partial T_e}{\partial r}\right) + P_{OH} - P_{line} - P_{Br} - P_{ion} + P_c^{eD} + P_c^{ep}, \quad (4)$$

$$\frac{3}{2}\frac{\partial(n_D T_D)}{\partial t} = \frac{3n_D}{2r}\frac{\partial}{\partial r}\left(\chi\, r \frac{\partial T_D}{\partial r}\right) + P_c^{De} + P_c^{Dp}, \quad (5)$$

$$\frac{3}{2}\frac{\partial(n_p T_p)}{\partial t} = \frac{3n_p}{2r}\frac{\partial}{\partial r}\left(\chi\, r \frac{\partial T_p}{\partial r}\right) + P_c^{pe} + P_c^{pD}, \quad (6)$$

where energy losses due to ionization (P_{ion}), Bremsstrahlung (P_{Br}) and line radiation ($P_{line} = \sum_i n_i n_e L_i(n_e, T_e)$) are considered as well as energy gain through Ohmic heating

($P_{\mathrm{OH}} = \sigma_{\parallel} E^2$). Line radiation ($P_{\mathrm{line}}$) is the sum of the radiation of each charge state n_i, which evolve due to electron impact ionization and the radiative recombination. The different particle species are coupled by the collisional energy exchange terms $P_{\mathrm{c}}^{kl} = 3n_k(T_l - T_k)/(2\tau_{kl})$, where the heat exchange time is $\tau_{kl} = \frac{3\sqrt{2}\pi^{3/2}\epsilon_0^2 m_k m_l}{n_l e^4 Z_k^2 Z_l^2 \ln\Lambda}\left(\frac{T_k}{m_k} + \frac{T_l}{m_l}\right)^{\frac{3}{2}}$. Heat diffusion is treated according to a simple diffusion model ($\chi = 1\mathrm{m}^2/\mathrm{s}$, averaged gyro-Bohm value). These equations are solved together with a model for the current decay and runaway electron generation in a runaway code [10].
As the plasma cools, its conductivity drops ($\sigma_{\parallel} \sim T_{\mathrm{e}}^{3/2}$), and a toroidal electric field is induced which keeps the current constant on time scales short compared to the current quench. The electric field is governed by the Maxwell equations and Ohm's law:

$$\frac{1}{r}\frac{\partial}{\partial r}\left(r\frac{\partial E}{\partial r}\right) = \mu_0 \frac{\partial}{\partial t}\left(\sigma_{\parallel} E + n_{\mathrm{run}} e c\right). \tag{7}$$

If the electric field exceeds the critical electric field ($E_{\mathrm{c}} = m_{\mathrm{e}} c/(e\tau)$) runaway electrons are produced. Two primary runway generation mechanism are considered in this study: Dreicer and hot tail runaway generation. This is an extension of our earlier studies, which only included the Dreicer runaway generation at a rate [10]:

$$\frac{dn_{\mathrm{run}}^{D}}{dt} \simeq \frac{n_{\mathrm{e}}}{\tau}\left(\frac{m_{\mathrm{e}}c^2}{2T_{\mathrm{e}}}\right)^{3/2}\left(\frac{E_{\mathrm{D}}}{E}\right)^{3(1+Z_{\mathrm{eff}})/16} e^{-\frac{E_{\mathrm{D}}}{4E} - \sqrt{\frac{(1+Z_{\mathrm{eff}})E_{\mathrm{D}}}{E}}}, \tag{8}$$

where $\tau = 4\pi\varepsilon_0^2 m_{\mathrm{e}}^2 c^3/(n_{\mathrm{e}} e^4 \ln\Lambda)$ and $E_{\mathrm{D}} = m_{\mathrm{e}}^2 c^3/(e\tau T_{\mathrm{e}})$. Hot tail runaway generation is calculated with an analytical model [11] by assuming an exponential temperature decrease, which gives the runaway rate:

$$\frac{dn_{\mathrm{run}}^{h}}{dt} \simeq -\frac{du_c}{dt}\frac{2u_c^2 \mathrm{H}(-du_c/dt)}{v/v_{T0}}\int_{u_c}^{\infty}\frac{e^{-u^2}u^2 du}{(v/v_{T0})^2}, \quad u^3 = \frac{v_c^3}{v_{T0}^3} + 3\mathrm{H}(t-t_0)\frac{n_{\mathrm{final}}}{n_0}\nu_0(t-t_0), \tag{9}$$

Here, v_c is the critical velocity corresponding to the critical electric field E_c, $u_c = u(v = v_c)$, H is the Heaviside function, ν_0 is the initial electron-electron collision frequency, n_0 is the electron density and v_{T0} denotes the initial thermal velocity of electrons.
The number of runaways is further enhanced by the avalanche mechanism at the rate [10]:

$$\frac{dn_{\mathrm{run}}^{\mathrm{a}}}{dt} \simeq n_{\mathrm{run}}\frac{E/E_{\mathrm{c}} - 1}{\tau \ln\Lambda}\sqrt{\frac{\pi\varphi}{3(Z_{\mathrm{eff}}+5)}}\sqrt{\left(1 - \frac{E_{\mathrm{c}}}{E} + \frac{4\pi(Z_{\mathrm{eff}}+1)^2}{3\varphi(Z_{\mathrm{eff}}+5)(E^2/E_{\mathrm{c}}^2 + 4/\varphi^2 - 1)}\right)}, \tag{10}$$

where $\varphi = (1 + 1.46\epsilon^{1/2} + 1.72\epsilon)^{-1}$ and $\epsilon = r/R$ denotes the inverse aspect ratio.

To calculate the number of hot tail runaways by Equation (9), the electron temperature should decrease exponentially. Therefore, in the first cooling phase, the evolution of the background plasma temperature was recast to an exponential function with the final temperature given by Equations (1) - (3) and with a characteristic time t_0 named homogenization time. The particle density also increased exponentially as $n \sim (1 - \exp(-t/t_0))$.

The current quench time must be short in order to successfully mitigate the large vessel forces that can be caused by halo currents. Aiming at current quench time calculation we have chosen pellets which reach the plasma center when they are completely ablated. As slow pellets are prone to generate runaways, Fig. 5 shows a simulation for a low velocity carbon pellet ($v_{\mathrm{p}} = 100$ m/s, $r_{\mathrm{p}} = 0.89$ mm, $1.3 \cdot 10^{20}$ particles) where we assumed a

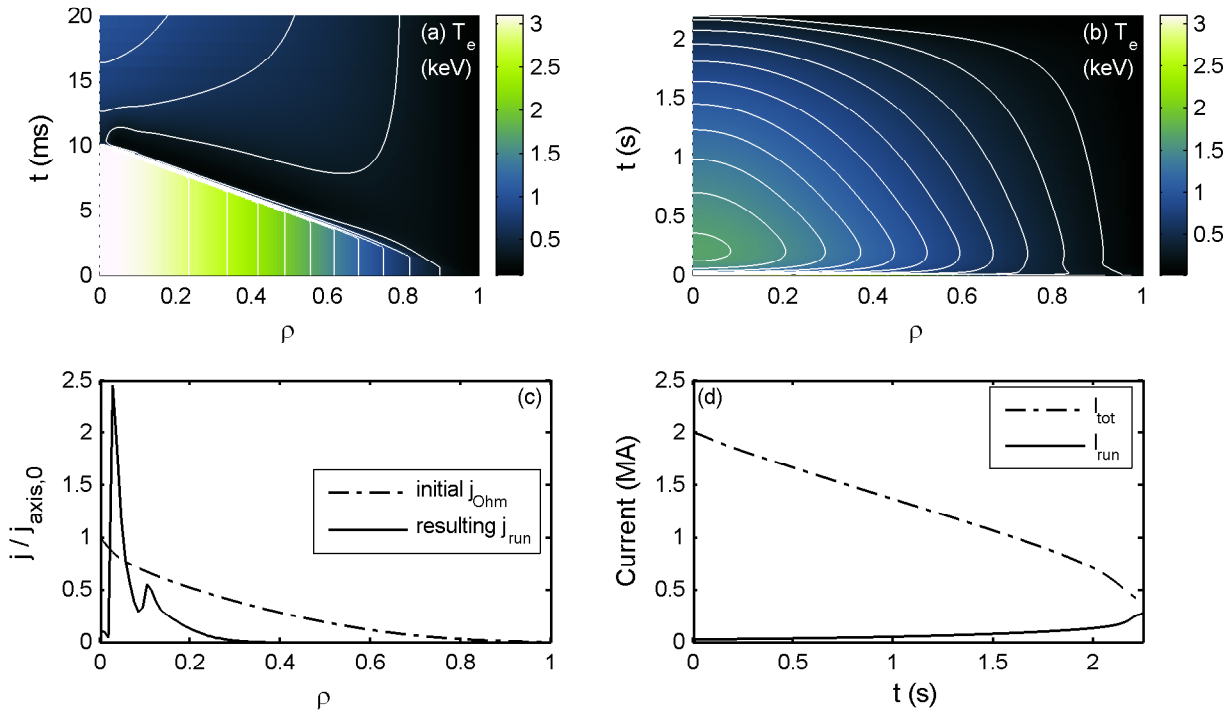

FIG. 5: A simulation of a carbon pellet with $r_p = 0.89$ mm ($1.3 \cdot 10^{20}$ particles) and $v_p = 100$ m/s. Evolution of the temperature on short (a) and long time scale (b). The density increase is too small to compensate for the temperature drop, so Dreicer and hot-tail runaways will be generated. (c) Initial radial profile of the Ohmic current density and the post-disruption runaway current density. (d) The total current falls on a slow time scale of several seconds, which gives the avalanche mechanism time to produce a considerable runaway current.

homogenization time of $t_0 = 0.5$ ms. During the current quench 14% of the initial plasma current has been transformed to runaway current, therefore carbon is not a good candidate to mitigate disruptions.

Due to large radiation losses, impurity pellets can cool the plasma considerably, but in the same time their injection might lead to runaway generation. Impurity doped deuterium pellets can combine the advantages of the deuterium and impurity pellets; they cool the plasma effectively, which shortens the current quench, and increase the density, which reduces the runaway generation. Therefore, a simulation with a carbon doped deuterium pellet ($r_\mathrm{p} = 1.6$ mm, v_p=1000 m/s) in a JET like plasma will be detailed here. In this case we assumed a particle homogenization time of $t_0 = 0.1$ ms. Fig. 6 shows the initial cooling caused by a pellet with 1% carbon. The red line denotes the initial electron temperature and the blue line shows the flux surface averaged temperature of the background plasma electrons when the pellet leaves its cloud. The pellet cloud has a cooling effect that can be several hundreds of electronvolts. The black curve on Fig. 6(a) shows the electron temperature after homogenization. The high ablation rate of the doped pellet will result a huge density increase (Fig. 6(b)).

Fig. 7 shows the simulated temperature change at $r/a = 0.5$. The initial high radiation cools the plasma during and after the homogenization, but as the carbon atoms become

fully ionized, the strong Ohmic heating starts to reheat the plasma. On this long time scale, only heat diffusion can compete with Ohmic heating and cool the plasma. As the temperature drops the electric field exceeds the initial critical field, but the density increases sufficiently to suppress runaway generation. However, the current quench time is too long, because of the Ohmic heating, see Fig 8. The sublimation energy of carbon is much higher than for deuterium, so the size of the carbon pellet needed in order to reach the plasma center is smaller than the required size of deuterium or carbon doped deuterium pellets. However, the carbon and carbon doped pellets both cool the plasma to low temperatures, but in the case of carbon doped pellets the electron density is strongly increased and no runaways are produced. Carbon pellets on the other hand give considerably lower density, and runaways can easily be produced. The temperature after the thermal quench caused by fast carbon pellets or carbon doped deuterium pellets is too high to lead to a sufficiently short current quench, even in the cases where no runaways are produced.

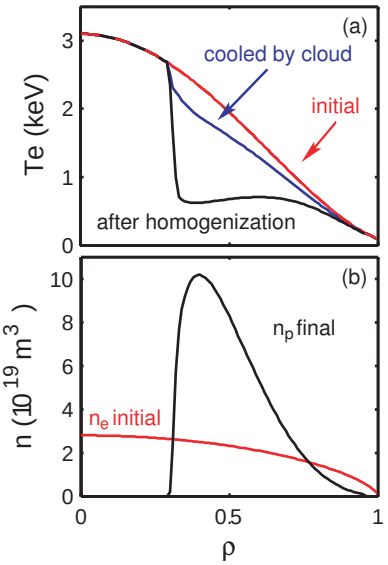

FIG. 6: The cooling and material deposition for a 1% carbon doped deuterium pellet with r_p = 1.6 mm, v_p=1000 m/s

4. Conclusion

The present work has shown that pellet injection is a promising tool not only for fuelling, but also for ELM and disruption mitigation. In present day devices such as ASDEX Upgrade and JET all injected deuterium pellets trigger ELMs. The pellet triggers an ELM before it reaches the pedestal top. The minimum particle content of pellets reaching

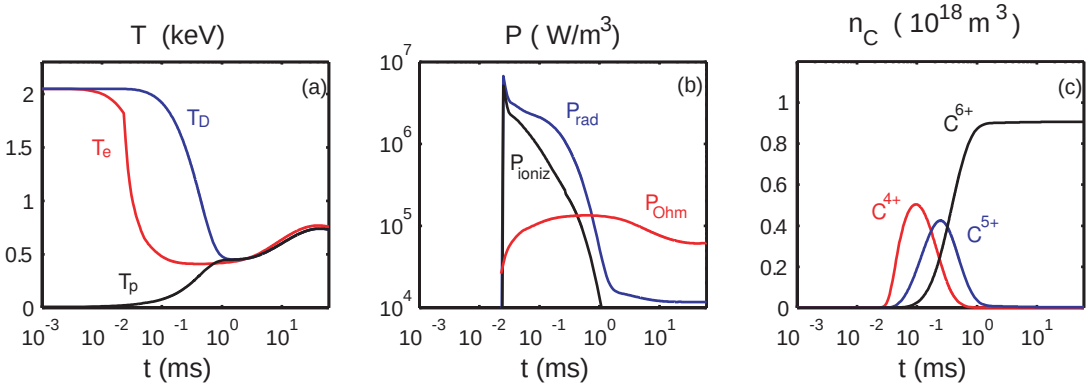

FIG. 7: Simulations for a 1% carbon doped deuterium pellet with v_p = 1000 m/s and r_p = 1.6 mm at $r/a = 0.5$. Time evolution of the (a) temperature of electrons, background ions and pellet ions; (b) of the radiation, ionization and ohmic heating power densities. The pellet enters the flux-tube at t=0. The power densities are shown after the time when the pellet has left the flux-tube at t = 0.02 ms. (c) The different ionization stages of carbon.

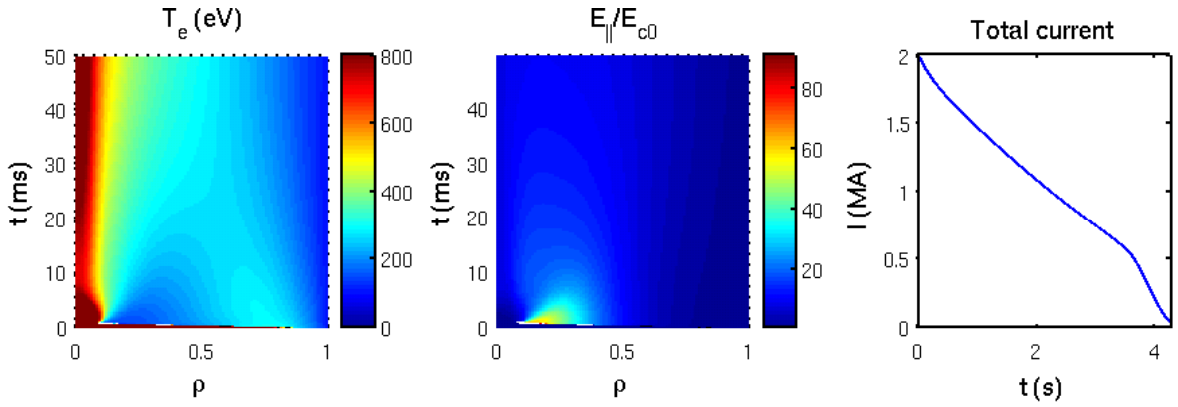

FIG. 8: A simulation of a carbon doped deuterium pellet with $r_p = 2.3$ mm and $v_p = 1000$ m/s and 1% carbon. The evolution of (a) the temperature, (b) the electric field (normalized to the initial E_c) on a short time scale and (c) the resulting current quench.

the pedestal top and triggering an ELM in ITER has been calculated for different pellet injection scenarios.

The strength of the density perturbation (deposited particles/m) that triggered ELMs in ASDEX Upgrade and JET experiments has been simulated. The minimum density perturbation required to trigger an ELM cannot be determined, since smaller and/or faster pellets than the presently technically available would have been needed. In all these experiments the density perturbation was of the order of 10^{20} 1/m, while for the pellets expected to trigger ELMs in ITER it is estimated to be an order of magnitude higher.

Different pellet injection scenarios were tested for disruption mitigation. To mitigate disruptions successfully by doped pellets the current quench must be much faster than what is obtained for carbon in this work, so deuterium pellets need to be doped by a higher Z material such as Neon or Argon, which is the subject of our ongoing studies. Both Dreicer and hot tail runaways are hoped to be suppressed by these pellets even in large devices such as ITER.

[1] Loarte, A., et al., Nucl. Fusion **47** (2007) S203.
[2] Lang, P. T., et al., Nucl. Fusion **44** (2004) 665.
[3] Chiu, S. C., et al., Nucl. Fusion **38** (1998) 1711.
[4] Gál, K., et al., Nucl. Fusion **48** (2008) 085005.
[5] Parks, P. B. and Turnbull J. R., Phys. Fluids **21** (1978) 1735.
[6] Lengyel, L. L., et al., Nucl. Fusion **39**, (1999) 791.
[7] Polevoi, A. R., et al., Nucl. Fusion **43**(2003) 1072.
[8] Lang, P. T., et al., Nucl. Fusion **47** (2007) 754.
[9] Lang, P. T. et al., Nucl. Fusion **48** (2008) 095007.
[10] Gál, K., et al., Plasma Phys. Control. Fusion **50** (2008) 055006.
[11] Smith, H. M. and Verwichte E., Phys. Plasmas **15** (2008) 072502.

This work, supported by the European Communities under the contracts of Association between EURATOM/HAS, VR, IPP, UKAEA and by the UK Engineering and Physical Sciences Research Council, was carried out within the framework of the European Fusion Development Agreement. The views and opinions expressed herein do not necessarily reflect those of the European Commission.